Catalysis Today 150 (2010) 308–318

Contents lists available at ScienceDirect

Catalysis Today

journal homepage: www.elsevier.com/locate/cattod

Simulation of light naphtha dimerization using a PtZrGa/Si mesoporous catalyst in a swing mode of operation

Roberto Galiasso Tailleur *, Cirlia Albornoz

Simon Bolivar University, Department of Thermodynamics, Sartenejas Caracas, Venezuela

ARTICLE INFO

Article history:
Available online 28 November 2009

Keywords:
Light naphtha
Dimerization
Swing reactor
PtZrGa/Si

ABSTRACT

A new process for selective dimerization of commercial cracked light naphtha (C_{4-6}) into gasoline-range molecules (C_{7-11}) was simulated. The reaction takes place at a low-hydrogen partial pressure in the presence of a $PtZrGaO_x/ZrSiO_y$ mesoporous catalyst. The apparent kinetic rates of reactions and deactivation models, previously determined in microplant tests, were confirmed with three experimental one-week tests. The kinetic for catalyst regeneration was then determined on these spent catalysts. The simulation results show that the use of two swing-axial gas-phase reactors operating in parallel but out of phase by one week produce the best economical cycle of operation. That occurred when the increase in temperature as function of time at the inlet of each bed follows a particular ratio. The regeneration of the spent catalyst by solvent and hydrogen recovers most of the activity and all the selectivity. The fresh, spent and regenerated catalysts' properties are briefly described.

1. Introduction

Refineries have shown interest in the last 10 years in converting the light naphtha produced in catalytic and thermal conversion processes into a gasoline-range component. The use of methanol and other lighter oxygenates provides incentives for the use of lower Reid vapor pressure for the gasoline components. This transformation must be oriented to produce high-octane (with relative high branching degree), low vapor pressure, and low aromatics content (stable) gasoline. Preliminary economical calculation shows the incentive for dimerization of light naphtha in spite of the reduction in volume associated with the C_4 and C_5 olefin conversion into higher molecular weight compounds and the existence of other options for the use of these types of feed.

Numerous studies of polymerization reaction mechanisms for C_{4-5} olefins – light naphtha components – have been published to date. Each of them is based upon a catalyzing agent that ultimately delivers a maximum amount of polymerized gasoline from light olefins. Lutz and Bailey [1] have studied the selective polymerization of 1- and 2-pentenes using a Ziegler Natta type of catalyst and determined an important difference in reactivity between the low olefins that generated high molecular weight polymers. Polyanski and Tsekhmister [2] reported the selective polymerization of pentenes on sulfonated resins into C_{10-14} compounds. Hochtl et al. [3] studied 1-pentene isomerization over several catalysts with varying acidity and found that the degree of isomerization, dimerization, cyclization, and cracking reactions is dependent upon the degree of acidity and other zeolite characteristics, but most of them present severe deactivation processes. Rutembeck et al. [4] described the isomerization mechanism of *n*-butene to iso-butene on SZM-5 zeolite, considering that isobutene is the most reactive in the formulation of gasoline. Two-stage dimerization of the C_{5-11} fraction to produce lube oil was claimed by Miller and Krug [5]. More recently, Schmidt et al. [6] oligomerized C_5 olefins present in light catalytic naphtha with high conversion using high silica/alumina ratio zeolites; in particular, they used a mordenite with relatively stable activity for almost 40 h on stream. In the abundant literature published in the last 20 years on the use of zeolites for pentane isomerization or dimerization, the common denominator is the high deactivation suffered by the acid catalyst when it is contacted with olefins. In our research group (Bonilla Platin and Galiasso Tailleur (1997)) [7], we developed a new mesoporous PtGaZr/ZrSi type catalyst and determined the apparent kinetics of reactions and deactivation using a particular light cracking naphtha (mainly C_5). We demonstrated that it is possible to obtain high conversion with moderate deactivation in the presence of hydrogen using a fixed-bed gas-phase reactor operating at mild conditions, a process that will be simulated here. A catalyst similar to, but less acidic (lower Ga content) than the present PtGaZr/Si, has been used for the isomerization of light naphtha (Galiasso Tailleur and Bonilla Platin (2008)) [8]. The benefits on selectivity and stability of acidity modulation by using

* Corresponding author. Current address: Department of Chem. Biol. & Mat. Engineering, Oklahoma University, Norman, OK 73019, United States.
Tel.: +1 4057950432; fax: +1 4053255813.
E-mail address: galiassor@ou.edu (R. Galiasso Tailleur).

0920-5861/$ – see front matter © 2009 Elsevier B.V. All rights reserved.
doi:10.1016/j.cattod.2009.10.013

Nomenclature

a	mass transfer area [m^2/m^3]
a	catalyst activity
$C_{j,g}$	gas-phase concentration
C_j^s	solid concentration [mol/L]
Cp_j	heat capacity [cal/mol K]
Da	Dankoeler number
ni	order of reaction [–]
D_{ef}	effective diffusivity [cm^2/s] 80 °C
d_p	particle diameter [m]
E_i	activation energy [kJ/mol]
E_d	deactivation energy [kJ/mol]
E_{reg}	regeneration energy [kJ/mol]
f	function [–]
F_j	molar flow [mol/h]
g	acc gravity
h	heat transfer in the film [cal/s]
H_i	enthalpies [cal/mol]
$k_{0,i}^{t=0}, k_{0,i}^{t=t}$	pre-exponential factor $[(mol/m^3)^{-nOl+nH_2}\ s^{-1}]$; reaction i at $t = 0$ and $t = t$
k_d	pre-exponential deactivation factor [1/day], acid site
k_{jlS}	mass transfer coefficient [m/s]
k_{reg}	apparent reg factor [d^{-1}]
L	characteristic length of catalyst [m]
nOl, nP	order for to olefins and paraffin Eq. (3) [–]
nH_2	order for hydrogen Eq. (3) [–]
r_i	reaction rate [$mol/m^3/h$]
r_i^{obs}	observed reaction rate [$mol/m^3/h$]
R	gas constant [J/mol K]
t	time on stream [d]
T	temperature [K], o: initial, t: other time
T_g	gas temperature [K]
T_s	solid surface temperature [K]
V	volume of the reactor
x	conversion [–]
Z	length of reactor bed [m]

Greek letters

δ	differential
$\varepsilon_{j,i}$	empirical stoichiometry [–]
Δ	delta
φ	Thiele module [–]
ρ	solid density [kg/m^3]
υ	volumetric catalyst fraction [m^3/m^3]

Subscripts

i	reaction
j	compound

Ga-Zr and Ga-Si acid sites instead of Al-Si was demonstrated. In addition, we demonstrated the role of Pt and the hydrogen partial pressure on controlling the deactivation in a radial gas-phase reactor. The catalyst deactivation [9] in oligomerization is always attributed to coke deposition, and most of the regeneration practice (for example Mariochionna et al. [10]) burned off these polymers to recover the activity and go out of stream for almost 20 days.

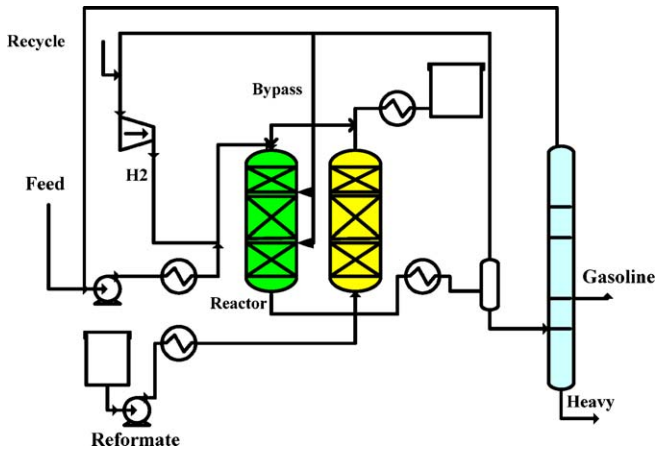

Fig. 1. Simplified process scheme. Two plug flow reactor operating simultaneously in parallel or out of phase. Two hydrogen quenches in each reactor.

Commercial light naphtha dimerization process is available through different companies like Lyondell (Marechioni et al.) [11] and UOP (Frame et al.) [12], among other suppliers of technologies. In addition, important works have been published on the simulation of gas-phase reactors. Chen et al. [13] modeled and simulated a fixed-bed reactor with pseudo-homogeneous two-dimensional flow, describing the dynamic and steady state behaviors of a light-cocker naphtha pilot-plant hydrotreater. Savoretti et al. [14] evaluated by simulation their non-adiabatic, radial flow fixed-bed reactor proposed to carry out the dehydrogenation of ethyl benzene to styrene. More recently, Lee and Froment [15] presented a kinetics analysis of ethylbenzene dehydrogenation into styrene, accounting for heterogeneous kinetic and mass transportation phenomena. The interesting possibilities of using swing reactors operating in gas phase were analyzed by Aida and Silveston [16], by Lee et al. [17] and Heidebrecht et al. [18], among others. To our knowledge, there is no model available for simulating the dimerization while accounting for deactivation and catalyst regeneration.

In this paper, we simulate the operation of swing (axial) adiabatic type reactors, having three packed beds of PtGaZr/ZrSi catalyst, using lumped kinetic and deactivation rate models already developed and new data for catalyst deactivation and regeneration. The catalyst and the mechanism of reaction, deactivation and regeneration were analyzed. A mathematical model was developed to look for the optimal operation in a one-year cycle based on minimizing the investment and operating cost of the plant (Fig. 1).

2. Experimental and model for simulation

2.1. Catalyst preparation

The catalyst was prepared in a Teflon-lined autoclave. Pluronic 123 was dissolved in 200 g of 2 M sulfuric acid blended under stirring with tetraethyl orthosilicate, gallium sulfate, and zirconium sulfate. The blend was kept at room temperature for 6 h; the reactor was then heated to 375 K and maintained at this temperature without agitation for 24 h. Subsequently, ammonium hydroxide was added to obtain a neutral pH and kept at 373 K for another 24 h. The produced solid was filtered, washed, dried, and extruded using the mother liquor as binder (5 wt%). The 1 mm × 5 mm extrudates were calcined in air at 573 K for 4 h and treated with steam and ammonium at 473 K for another 3 h. The solid was subsequently impregnated with an aqueous solution of Pt diamine-chloride compound at room temperature, dried, and

Table 1
Fresh, spent[a] and regenerated[b] catalyst properties.

Properties	Fresh	Spent	Regenerated
Surface area (m^2/g)	180	113	145
Pore volume (cm^3/g)	0.47	0.33	0.42
Micropore vol. (cm^3/g)	0.12	0.01	0.07
Carbon content (wt%)	–	4.5	0.8
Relative acidity (mol 10^2/g)	12.5	2	7.42
Relative CO adsorption (–)	1	0.56	0.88
iC_5 Diffusivity[c] ($10^5\,cm^2/s$)	1.23	0.87	1.1
Activity (–)	1	0.74	0.92
Selectivity ($C_{7-10}/\Delta C_5$) (–)	85	80	84

[a] 470 K, one week isothermal operation.
[b] 350 K, 5 h regeneration.
[c] Effective diffusivity measured at 80 °C with iC_5 [23].

calcined in air at 673 K for 6 h. The catalyst was then activated in situ by hydrogen to control the reduction and dispersion of Pt, and its properties are shown in Table 1 (fresh).

2.2. Catalyst deactivation

First, 60 g of catalyst was loaded into a fixed-bed reactor and reduced under pure hydrogen at 573 K for 6 h at 0.8 MPa. Next, commercial light naphtha (see composition in Table 2) was treated for seven days operating isothermally at 430, 450, or 470 K at a space velocity of 1.0 h^{-1} and pressure of 0.8 MPa using a H_2/HC ratio of 0.022 (mol). The effluent of the reactor was analyzed by GC (HP5890, using a silver trap for olefins retention, connected through a splitting device to a 10 m-long PIONA capillary column). The GC was connected to a Philips 2250 Mass Spectrometer. Due to the difficulty in identifying all C_{11}^+ di- and tri-isomers by GC, their ratio mono-/di-branched paraffins were calculated at their thermodynamic equilibrium. This analysis was complemented by ^{13}C NMR analyses of the products to determine the average isomerization ratio ($isoC_i/nC_i$) using the shift and the ratio of CH/CH_3. Octane numbers were calculated using the Nikolaou et al. [19] correlation and the GC and ^{13}C NMR data. The catalyst was deactivated over a week, then the microreactor was cooled to room temperature, and the catalyst was downloaded from the reactor under inert atmosphere. The deactivation tests, performed isothermally at three different temperatures, generated after one week of continuous operation three spent samples that were characterized. Their activities were 0.91, 0.87 and 0.74; it is these tests that provide samples for catalyst regeneration and data to confirm kinetics and deactivation parameters. Samples of 15 g of each of the spent catalysts were set aside, and the rest was divided into portions (15 g) for regeneration. Each of the latter portions of catalyst was loaded into the same reactor used for deactivation, diluted with three volumes of inert material, and regenerated by the procedure described below. After the regeneration, the catalysts were tested at the operating conditions used during the deactivation to verify their activity (C_5 conversion) and selectivity (production of C_{7-10}/C_{10}^+, ratio by mol).

2.3. Catalyst regeneration

Each sample of the spent catalysts was regenerated by recirculation of xylene at 315, 335, or 355 K, at a space velocity of 1 h^{-1} over 6 h (0.8 MPa). The xylene stream was analyzed as a function of time to control the extraction. This adsorbed-compound leaching process was followed in all samples by a common hydrogen treatment (rejuvenation) at 773 K and 0.8 MPa pressure, for 10 h in countercurrent operations. Then the activity of the regenerated sample was tested by treating light naphtha at the operating conditions used for deactivation. In parallel, and for the purposes of characterization, 4 g of each sample were regenerated by xylene washing and hydrogen treatment in a microreactor at the same conditions described above, taking 1 g sample of partially regenerated catalyst each hour for characterization. The analyses of xylene extracts and the solids allowed us to determine the rate of carbon (hydrocarbons) removal for different xylene contact times and temperatures. Spent and regenerated catalysts were characterized by ^{13}C NMR, IR, and elemental analysis. The spent and regenerated catalysts were tested in the presence of light cracked naphtha at 450 K, 0.8 MPa, and 1 h^{-1} in a microplant reactor to determine the recovery of the catalyst activity and selectivity (Table 2).

2.4. Catalyst characterization

The pore structure of the three spent and regenerated catalysts was measured using nitrogen sorption experiments and BET or BJH analysis. The measures were performed in a Micromeritics ASAP 2010 apparatus at 70 K. The concentrations of carbon, sulfur, and hydrogen were determined by an elemental analyzer (EAI 4040). Sulfur was measured to control sulfur accumulation from the feed. IR spectroscopy of the catalysts was measured on a Perkin Elmer FTIR with DGS using a specially designed cell and an ultra-thin film (0.1 mm) hung on a quartz spring (Mc Bain thermo-balance). The solids were dried, degassed, and contacted with pyridine in argon at room temperature. The cell was heated to 423 K in argon, and the acidity was evaluated using the areas of the pyridine bands of adsorption (IR) that remain adsorbed, in the region of 800–1200 cm^{-1} (see detail in reference [8]). The Pt metal dispersions were evaluated by CO adsorption in the same IR cell at 700 Pa and 150 K using a methodology previously developed to measure the area of the bands at 2009 cm^{-1} (ν(C–O): Pt^0–CO) to compare the fresh spent and regenerated catalysts. The results were validated by TEM analyses (Table 1 shows the summary of catalysts properties).

Table 2
Selectivity (mol% on fresh feed) as for fresh, spent and regenerated catalysts H_2/HC: 0.06 (mol), *T*: 450 K, *P*: 0.8 MPa (~50% conversion).

Properties (mol/100 mol of feed)	Feed[a]	Fresh	Spent	Regenerated
Activity	–	1	0.84	0.96
C_3 (cracking)	–	1	0.3	1.1
nC_4/iC_4	1.0/0.4	0.3/0.0	0.7/0.3	0.3/0.0
$nC_5^=/iC_5^=$	36/13	1.2/0.1	1.4/0.1	1.3/0.1
nC_5/iC_5	35/10	6.0/2.7	8.0/4.0	6.3/3.0
$nC_6/iC_6/iiC_6$	0.5/0.3/0.0	0	0	0
$nC_7/iC_7/iiC_7$	0.0/0.0/0.0	0.2/0.5/0.3	0.17/0.4/0.25	0.23/0.55/0.1
$nC_8/iC_8/iiC_8$	0.0/0.0/0.0	0.9/1.5/0.7	0.86/1.4/0.65	0.8/1.45/0.65
$nC_9/iC_9/iiC_9$	0.0/0.0/0.0	0.9/1.75/0.87	0.85/1.7/0.82	0.85/1.7/0.82
$nC_{10}/iC_{10}/iiC_{10}$	0.0/0.0/0.0	6.1/19/6	5.7/18.0/4.8	6.0/18.8/5.6
C_{11}^+	0.0	5	4.6	4.9

[a] Commercial feed was pre-fractionated to reduce C_4 and C_6 content and sweetened to control the sulfur below 1 ppm; iC_5 and iiC_5 correspond to mono- and di-branched paraffins. The product does not include C_3 formed.

Table 3
Lump of reactions and kinetic parameters for the main reactions.

P	Lump of reactions Direct: $k_{io}E_i$/reverse: $k'_{io}E'_i$	k_{io}/k'_{io}	E_i/E'_i kJ/mol	n_{Ole} (–)	n_{H_2} (–)
1	$nC_5^= + nC_5^= \rightarrow nC_{10}^=$	3.10E+07 $h^{-1}(m^3/mol)^{nOl+nH_2}$	50.2	1	0
2	$iC_5^= + nC_5 \rightarrow iC_{10}^=$	2.50E+08 $h^{-1}(m^3/mol)^{nP+nH_2}$	55.76	1	0
3	$iC_5^= + iC_5 \rightarrow iiC_{10}^=$	5.60E+08 $h^{-1}(m^3/mol)^{nOl+nH_2}$	58.57	1	0
4	$nC_4^= + nC_4^= \rightarrow iC_8^=$	8.00E+06 $h^{-1}(m^3/mol)^{nP+nH_2}$	46.02	1	0
5	$iC_4^= + nC_4 \rightarrow iC_8^=$	3.00E+07 $h^{-1}(m^3/mol)^{nOl+nH_2}$	50.2	1	0
6	$iC_4^= + iC_4 \rightarrow iiC_8^=$	1.60E+08 $h^{-1}(m^3/mol)^{nP+nH_2}$	55.11	1	0
7	$nC_4^= + nC_5^= \rightarrow nC_9^=$	1.00E+06 $h^{-1}(m^3/mol)^{nOl+nH_2}$	37.65	1	0
8	$iC_4^= + nC_5 \rightarrow iC_9^=$	1.80E+07 $h^{-1}(m^3/mol)^{nP+nH_2}$	48.2	1	0
9	$iC_4^= + iC_5 \rightarrow iiC_9^=$	3.38E+07 $h^{-1}(m^3/mol)^{nOl+nH_2}$	50.11	1	0
10	$nC_8^= + nC_5^= \rightarrow nC_{13}^=$	3.00E+06 $h^{-1}(m^3/mol)^{nP+nH_2}$	48.34	1	0
11	$nC_8^= + iC_5 \rightarrow iC_{13}^=$	7.20E+06 $h^{-1}(m^3/mol)^{nOl+nH_2}$	50.23	1	0
12	$iC_8^= + iC_5 \rightarrow iiC_{13}^=$	1.50E+07 $h^{-1}(m^3/mol)^{nP+nH_2}$	52.65	1	0
13	$nC_8^= + nC_4^= \rightarrow nC_{13}^=$	3.20E+06 $h^{-1}(m^3/mol)^{nOl+nH_2}$	48.34	1	0
14	$nC_8^= + iC_4 \rightarrow iC_{13}^=$	7.20E+06 $h^{-1}(m^3/mol)^{nP+nH_2}$	50.23	1	0
15	$iC_8^= + iC_4 \rightarrow iiC_{13}^=$	2.50E+07 $h^{-1}(m^3/mol)^{nOl+nH_2}$	52.65	1	0
16–27	Trimerization reactions for C_9 and C_{10} with C_5 and C_4 hydrocarbons have the same rate constants (k_{io}, E_i) than C_8 with C_5 and C_8 with C_4 hydrocarbons. Reactions of di-branched olefins are neglected. Cracking reactions neglected.				
28	$nC_5^= + H_2 \leftrightarrow nC_5$	3.0E08/ 8.0E02 $h^{-1}(m^3/mol)^{nH_2}$	71.128/ 29.288	1 1	0.5 0
29	$iC_5^= + H_2 \leftrightarrow iC_5$	2.0E0.7/ 4.0E02 $h^{-1}(m^3/mol)^{nH_2}$	62.76/ 20.920	1 1	0.5 0
30	$nC_5^= + H_2 \leftrightarrow nC_5$	3.0E08/ 8.0E02 $h^{-1}(m^3/mol)^{nH_2}$	71.128/ 29.288	1 1	0.5 0
31	$iC_4^= + H_2 \leftrightarrow iC_4$	1.8E0.7/ 5.7E02 $h^{-1}(m^3/mol)^{nH_2}$	68.362/ 24.920	1 1	0.5 0
32	$nC_j^= + iC_j^= + iiC_j^= + yH_2 \leftrightarrow nC_j + iC_j + iiC_j$ for $j = 8, 9, \ldots, 15$	3.0E11/ 1.1E07 $h^{-1}(m^3/mol)^{nH_2}$	87.874/ 46.02	1 1.	0.5 0

2.5. Model simulation

2.5.1. Kinetic rate expressions and parameter

The experimental work of Bonilla Platin and Galiasso Tailleur [7], described in complementary information, showed that it is possible to simulate the complex set of reactions and deactivation involved in dimerization–trimerization using a lump of 50 reactions and found values of apparent kinetic and deactivation rate parameters. The previous data was obtained in three sets of 30 days continuous catalyst testing using as feeds blends with different concentrations of C_4, C_5 and C_8 (*n*-paraffin, one iso-paraffin, *n*-olefins and one iso-olefins), and C_{10} (*n*-decane and 1-decene) hydrocarbons diluted in Decalin. Temperatures, H_2/HC ratio, and residence time were varied at three levels to obtain 135 different experimental data points. This information was processed using a simulation program that has a genetic algorithm (GA) optimization tool (complementary information shows the flow scheme of the program in Figure 8). The inputs of the program were the equations for the rate of reactions and deactivation, the operating conditions, the mass balance for a plug flow isothermal reactor model and the value of the kinetics and deactivation parameters. The program reports the founded kinetics and deactivation parameters that fit the data at ±1%. These parameters were verified using the same program to predict the C_5 conversion and C_{10} normal and isoparaffin content in the products obtained in the dimerization of three other commercial naphthas (complementary information, Figure 9) in the range of 60–90% conversion.

In the present work, three additional one-week catalyst deactivation tests were performed using light naphtha with small amounts of C_4 and C_6 content and without diluents. The previous kinetics and deactivation parameters were (Table 3) together with the computational programs to simulate the activity (C_5 conversion), selectivity (C_{7-10}/C_{10}^+) and average activity of the bed as a function of time. The simulation considered the daily operating conditions, the orders of reactions, the pre-exponential factors (k_{oi}, $k'_{o,i}$, k_d), and the activation energies (E_i, E'_i, E_d). The comparison between the concentration of nC_{10} predicted and the average iC_i/nC_i ratio versus the experimental values are shown in Fig. 3.

The main assumptions used by the simulation model were:

- Thermal cracking, cyclization, trimerization and aromatization reactions were neglected based on the GC–MS analysis that shows very small amount of light hydrocarbons, cycloparaffins, and C_{15}^+ heavy products formed;
- All different iC_{7-11}, iiC_{7-11} and $iiiC_{7-10}$ isomers measured by GC are lumped into mono- and di-branched isomer families per atom of carbon (*j*: 7, 8, …, 11). All the isomer for iC_{11}^+, iiC_{11}^+ and $iiiC_{11}^+$ are measured together due to the severe overlapping in the GC analysis and the distribution between isomers are considered at the equilibrium

$$iC_{11}^+ \Leftrightarrow iiC_{11}^+ \Leftrightarrow iiiC_{11}^+ \quad \text{At equilibrium} \tag{1}$$

- dimerization and trimerization are irreversible reactions, while those of hydrogenation are reversible reactions;
- hydrogenation reactions for the $C_7^=+$ olefins, isoolefins, and cycloolefins are so fast that all can be lumped together into one rate of reaction, despite their differences in molecular weight.

The apparent reactions selected represent a very complex mechanism of C_5 dimerization reactions that involve the formation of adsorbed carbonium ($nC_i^+, iC_t^+, iiC_i^{++}$) species. The path of reactions starts with the formation of olefins and then the carbonium (Eqs. (2)–(5)) followed by their isomerization. These adsorbed species are then dimerized (Eqs. (6)–(8), and other combinatorial with different carbonium species) that produce different concentrations of $iC_{10}^+ + iiC_{10}^+ + iiiC_5^+ \ldots$ on surface. This dimeric carbonium can react with any other carbonium on surface (Eq. (9)) to produce a trimer or desorb to produce olefins (for

example Eq. (10)) or cracked (for example Eq. (11)); the olefins are hydrogenated on metal site (12) or start again to recombine with other molecules, and so on. In addition, the adsorbed carbonions species might dimerize and cyclisize into cyclo-carbonium ion (acC_5^+ – intermediaries) that might desorb to produces cycloolefins (14) and then be hydrogenated on metal site, or polymerize and dehydrogenate into coke precursors (15). The *i*: 7, 8, ..., 10 isomers may not be at the equilibrium.

$$nC_5 \overset{-H_2}{\longleftrightarrow} nC_5^= \rightarrow nC_5^+ \Leftrightarrow iC_5^+ \Leftrightarrow iiC_5^+ \ldots \quad (2)$$

$$iC_5 \overset{-H_2}{\longleftrightarrow} iC_5^= \rightarrow iC_5^+ \Leftrightarrow iiC_5^+ \ldots \quad (3)$$

$$nC_5^= \rightarrow iC_5^+ \Leftrightarrow iiC_5^+ \ldots \quad (4)$$

$$iC_5^= \rightarrow iC_5^+ \Leftrightarrow iiC_5^+ \ldots \quad (5)$$

$$nC_5^+ + nC_5^+ \rightarrow iC_{10}^+ \Leftrightarrow iiC_{10}^+ \ldots \quad (6)$$

$$iC_5^+ + nC_5^+ \rightarrow iiC_{10}^+ \Leftrightarrow iC_{10}^+ \ldots \quad (7)$$

$$iC_5^+ + iC_5^+ \rightarrow iiiC_{10}^+ \Leftrightarrow iiC_{10}^+ \ldots \quad (8)$$

$$nC_{10}^+ + nC_5^+ \rightarrow iC_{15}^+ \Leftrightarrow iiC_{15}^+ \ldots \quad (9)$$

$$nC_5^+ + nC_5^+ \rightarrow iC_{10}^+ \Leftrightarrow iiC_{10}^+ \ldots nC_{10}^+ \quad (10)$$

$$iC_{15}^+ \rightarrow iC_5^+ + nC_{10}^+ \ldots \quad (11)$$

$$nC_{10}^+ \overset{+H_2}{\longleftrightarrow} nC_{10}^= \quad (12)$$

$$iC_5^+ + iC_5^+ \Leftrightarrow acC_5^+ \quad (13)$$

$$acC_5^+ \rightarrow acC_5^= \quad (14)$$

$$acC_5^+ + acC_5^+ \overset{-H_2}{\longrightarrow} \text{coke precursor} \quad (15)$$

These large numbers of potential steps involved in the production of many compounds were simulated by using a simplified set of apparent homogeneous reactions depicted in Table 3. There the carbonium concentrations on the surface are represented by the gas-phase concentration of the paraffins and olefins. In particular, the production of *n*-paraffins with carbon number *j*: 7, 8, ..., 15 can be explained by cracking reactions (Eq. (11)) or by fast isomerization of isoparaffins and hydrogenation. Due to the narrow distribution of carbon number and the small amount on heavy paraffins observed in the reaction products (mainly iC_{10}), instead of using type (6) equations the model employs empirical dimerization equations between adsorbed $nC_5^=$ to produce $nC_{10}^=$ (Table 3, for reactions 1, 4, 7, ..., 25), paths that are not supported by the acid carbenium ion mechanism of reaction, but simplified the calculations. Therefore, fast adsorption–desorption of hydrocarbons, as well as fast hydrogenation–dehydrogenation reactions and a very low rate of cracking, were assumed. The order one, used for dimerization and trimerization reactions with respect to hydrocarbons, assumes that the rate-controlling step is the reaction of the adsorbed carbonium intermediaries. The apparent 0.5 order with respect to hydrogen is an empirical result (originally order 0 was proposed base on isomerization studies) and could not be explained by a simple mechanistic analysis; the hydrogenation and dehydrogenation reactions are relatively fast at present operating conditions. This apparent order for hydrogen was calculated from three independent experiments at different hydrogen partial pressure performed with the catalyst at different deactivation times and might include other effects.

During the previous kinetics study a 50/50 blend of 1-decene and 1-pentene was tested (450 K, 1 h^{-1}). It was observed that the conversion of 1-decene into C_{15} was negligible while most of the pentene was dimerized and hydrogenated into iC_{10}. When only 1-decene was used in the feed, nearly 20% of iC_{10}, 10% of cracked product and C_{15}^+ hydrocarbons were obtained at the same operating conditions. All of this confirms the preferential adsorption of the C_5 intermediary, the low cracking rate and the fast hydrogenation of C_{10} olefins. The model predicts the normal, mono- and di-branched hydrocarbons production using the following apparent pseudo-homogeneous kinetic rate equations ((16) and (17)).

$$r_i = k_{0,i}^{t=0} a \exp\left(\frac{-E_i}{RT}\right) C_j^{n\mathrm{Ol}} C_j^{n\mathrm{P}} \quad i: 1, 2, \ldots, 27; \quad (16)$$

$$r_i = k_{0,i}^{t=0} \exp\left(\frac{-E_i}{RT}\right) C_j^{n\mathrm{Ol}} C_{13}^{n\mathrm{H_2}} - k'_{o,i} t = 0 \exp\left(\frac{-E'_i}{RT}\right) C_j^{n\mathrm{P}}$$
$$i: 28, 29, \ldots, 32 \quad (17)$$

2.5.2. Catalyst deactivation model

The catalyst contains two types of active sites: one is responsible for the hydrogenation–dehydrogenation of olefins and paraffins (Pt), and other, for the isomerization, dimerization, trimerization, cyclization (Ga-Zr) and cracking. We have demonstrated [8] that on this type of catalyst the metallic sites, due to fast hydrogenation–dehydrogenation, do not modify the activity and selectivity of the acid sites but control the catalyst deactivation. Paraffins and olefins only dimerize and isomerize on acid sites [8], but at the same time it produces small amounts of cycloparaffins, coke precursors (xylene-soluble) and coke. In this model, instead of considering a mechanistic equation ((14) and (15)) for acid site deactivation that depends on cyclo-intermediary carbonum concentration, we have modeled the deactivation by one empirical equation using the Levenspiel [20] approach. That allowed us to define the same deactivation function for all the dimerization and trimerization reactions as a function of level of activity, time on stream, total olefin concentration, temperature, and hydrogen partial pressure. This equation was selected based on the deactivation results obtained by Galiasso Tailleur and Davila [21] in a naphtha reforming commercial test:

$$-\frac{da}{dt} = k_d e^{(-E_d/RT)} a \left(\frac{C_{\mathrm{Olefin}}^{C_4^= + C_5^=}}{1 + 0.2 e^{(1500/RT)} C_{\mathrm{H_2}}}\right), \quad (18)$$

$$a = \frac{k_{0,i}^{t=t}}{k_{0,i}^{t=0}} \quad \text{for } i: 1, 2, \ldots, 21 \quad (19)$$

The initial activity for fresh catalyst is 1; the catalyst deactivation constant k_d was found in a previous study to be 1×10^{17} day^{-1} and the deactivation energy E_d is 158.99 kJ/mol [7]. Pt deactivation is relatively slow and it is disregarded.

2.5.3. Catalyst regeneration model

The regeneration of the catalyst occurred by washing the weakly adsorbed coke-precursor hydrocarbons that cover the active sites and then hydrocracking of the remaining strongly adsorbed molecules (on acid and metal sites). These condensed dehydrogenated products, generated from the cyclo-intermediaries, would progressively age and become insoluble coke. The regeneration procedure recovers both, the active acid and metal sites (Table 1). The simulation of the recuperation of the catalyst activity can be modeled by a simple

equation [20]:

$$-\frac{da}{dt} = k_r e^{(-E_r/RT)}(1-a), \tag{20}$$

where the activity was defined according to Eq. (19).

The rate of regeneration is simplified to be a function of the level of activity (number of active acid sites blocked for the reaction), time and temperature of operation, but independent of the concentration of adsorbed cyclo-intermediaries.

2.5.4. Thermodynamic properties

The specific heats of reactions used here were as follows: for hydrogenation: −41.84 kJ/mol H_2; for dimerization: 20.92 kJ/mol of olefin; and for isomerization of olefins: −5 J/mol. Heats of reactions were considered independent of temperature in the range of 400–480 K used here. The specific heat capacities for the gases were evaluated using the conventional equation for components (21) and for the blend using their molar contribution (22):

$$C_{pi} = A + BT + CT^2, \tag{21}$$

$$C_{p,m} = \sum x_i C_{p,i} \tag{22}$$

A, *B* and *C* are the constants reported in the thermodynamic handbooks. The vaporization of all the components was verified by performing an adiabatic flash at 0.8 MPa, 0.03 H_2/HC, and 400–450 K in PROII (Provision II, Peng Robinson state Equation) to verify that the heavy (C_{10}–C_{15}) molecules produced are still in the gas phase. The results confirm the presence of almost 10% of liquid at high olefin conversion, a number that decreases when the additional hydrogen is added in the quench. The following development assumes that only gas phase is present in the reactor nevertheless additional fluid dynamic studies are ongoing to evaluate the effect of liquid formation in the axial reactor performances.

The equilibrium constants for the isomerization of C_{11}^+ paraffins were calculated based on the Pellegrini et al. [22] published correlations. Notice that the value of equilibrium constants for mono to poly-branched paraffins for C_{12}–C_{15} hydrocarbons (450 K) goes from 7 to 27 (mol/mol) as the carbon number increases, therefore the C_{11}^+ hydrocarbons contain mainly branched paraffins. Effective diffusivity in fresh, spent, and regenerated catalyst was measured with isopentane in a shallow bed reactor as it was described in a previous paper [23] (Table 1).

2.5.5. Mass and heat balance

In a plug flow axial reactor, the mass balance provides the following general equation for the *j* component, and *i* reaction:

$$k_{LS}a(C_j^g - C_j^s) = \upsilon\sum_{j=4}^{15}\eta_j\varepsilon_{j,i}r_i = \frac{dF_j}{Adz} \tag{23}$$

The energy balance is as follows:

$$\frac{udT}{dz} = \frac{h_s a(Ts - T)}{\sum \rho_L C\,p_L} = \frac{\upsilon\sum \eta_j\varepsilon_{j,i}r_i(-\Delta H_i)}{\sum \rho_L C\,p_L}\Bigg) \tag{24}$$

The rate of catalytic reactions must consider the mass and heat transfer rates in the bed, in gas film surrounding the particle, and in the pores. To be able to account for or to neglect these effects, several dimensionless numbers must be calculated to verify their relative importance in the model (well described in specialized books [24]). Mass transfer rate control of the reaction in the film and in the pores was evaluated by calculating the Dankohler (25) and Thiele (26) numbers for the highest rate of reaction in the system.

$$Da: \frac{r_i^{obs}}{kgC_{j,g}^{obs}}, \tag{25}$$

$$\varphi: \frac{1}{L}\sqrt{\frac{r_i^{obs}}{D_{ef}C_{j,g}^{obs}}} \tag{26}$$

Resistance to heat transfer in the film was evaluated by:

$$(T_g - T_s) = \frac{L(-\varepsilon_{j,i}r_{i,obs})(-\Delta H_r)}{h} \tag{27}$$

The mass and heat transfer rates were calculated using the highest observed rate of reactions (r_i^{obs}). The model is able to solve the mass and heat balance equations including the mass transfer and heat transfer rates.

2.5.6. Numerical method and methodology

A fourth-order Runge–Kutta–Fehlberg numerical method was used to solve the set of mass and heat balances differential equations ((23) and (24)). The program written in VB™ 6 read the inlet operating conditions and the mode of operation of the reactor (isothermal, adiabatic, or programmed temperature profile), calculated the required thermodynamic constants values, and began solving the mass and heat balance differential equations point by point along the first catalytic bed volume. On the first day of operation, the catalyst activity was equal to 1, and the program calculates the conversion and temperature along the first reactor bed volume until it reaches the maximum delta of temperature specified by the user. At this point, the program adds cold hydrogen (quench) to reduce the gas temperature to the level specified by the user, and continued calculating the concentration and temperature profiles along the second reactor bed. Again, when the maximum delta of temperature is achieved in the second bed, additional amount of hydrogen is added to recover the inlet gas temperature for the third bed. After that, the program calculates the concentration and temperature along the third bed reactor volume until it reaches the maximum delta of temperature or the conversion level. In this way, the calculation for the first day in operation is finished. Next, the program increases the time on stream according to specification (for example three days) and recalculates the profile of activity using Eq. (18), and then temperature, hydrocarbons and hydrogen concentrations along the three beds with the new profile of catalyst activity. The two hydrogen quenches were added in the same point (reactor volume) as calculated for the first day of operation. If the outlet concentration is not able to fulfill the conversion specified by the user, the program increases the inlet temperature of the three beds until this conversion is achieved. The program continues calculating the activity profile along the time on stream by increasing the inlet temperature following a specified pattern defined by the user until the average activity dropped below certain value or arrived to the maximum temperature at any place in the reactor. At this moment, this reactor is switched into a regeneration mode and the second reactor is put on stream. The latter reactor operated while the catalyst in the first reactor was regenerated. The user can also decide to work with a single reactor at a time or two, operating in parallel but out of phase in time (for example, by one week). The program is able to calculate the operational time required for regenerating the catalyst based on its activity at the end of run to minimize the off-stream time for the reactors and maximize the production. At the end the program performs a general mass balance to calculate the investment, operating cost and gross benefits per unit of product ($/bbl). Table 4 summarizes the input and output of the model.

Table 4
Program input and output for simulation the mode of operation.

Input	Output
Molar flow of components C_{1-15} and H_2	Molar flow of products C_{1-15} and H_2
T inlet temperature	Profile of temperature along the reactor
Pressure and H_2/HC ratio	Profile of concentrations along the reactor
Rate constants and order of reactions	Amount of H_2 in quenches
Deactivation constants	Profile of activity in reactor cycle
Regeneration constants	Profile of activity during regeneration
Heat of reaction, *Cp* and other properties	Cost of reactor
Number of reactor in operation	Cost of the plant
Mode of operation	Gross benefits for a one-year cycle operation
Cost of utilities, feed and products	Cash flow for one-year cycle operation
Engineering index, location factor	Time on stream

2.5.7. Gross benefits

The yearly gross benefits (GB: ($/y products–$/y feed–$/y operating cost)) were calculated based on a general mass balance for the plant, the dimension of the reactor and other equipments in the plant, the product and the utilities required for one year operation. Here, only the results of the GB calculation will be shown for a plant located in the Gulf Coast in 2004, with 17-year depreciation before tax. The aforementioned program provided the yield of the unit and the naphtha and hydrogen consumption over one year of cycle operation. Then it calculated the earnings and expenses at fixed annual production. Octane number of the product was calculated using a correlation based on composition (complementary information – Figure 11 octane number comparison between predicted and measured value in dimerized naphtha). The price of the equipment was obtained from Oracle™ data base.

3. Results

3.1. Catalyst characterization

Table 1 shows the properties for fresh, spent, and regenerated catalysts.

3.1.1. Fresh catalyst

Fresh catalyst is a mesoporous material with a surface area of 180 m^2/g (lower than a mordenite zeolite), a pore volume of 0.51 cm^3/g, and a small microporous volume ($d_p < 1$ nm). TEM analysis of the solid shows an open porous structure with larger openings than the 6–8 Å measured in mordenite. The chemical analysis indicated that the catalyst contains a SiO_2/Ga_2O_3 ratio of 10, a SiO_2/ZrO_2 ratio of 14 (wt), and 0.3% of Pt. The metal loading is lower than commercial Pt/mordenite isomerization catalyst (not shown), and the catalyst used here has (TEM and CO adsorption measurement) high metal dispersion (31% dispersion, average particle diameter of 16 Å in clusters). The fresh catalyst did not present appreciable amounts of coke, and it adsorbed twice as much pyridine at 500 K than did mordenite Si/Al 40 (not shown). Table 3 shows an example of activity and selectivity of the fresh catalyst at 450 K. Since the current feed is mainly composed of C_5 hydrocarbons, most of the product is C_{10}, with small amounts of C_{7-9} and C_{11-14} associated to C_4 conversion, trimerization and catalytic cracking of dimers and trimers produce C_3 not included in the model. The iC_i/nC_i ratio is around 3.5 (average value in whole C_{7-15} product), which slightly decreases with the increase in temperature, as well as the octane number. The most abundant iC_{10} hydrocarbons are: $2MC_9$ and $3MC_9$ and the iiC_{10} are: 2,5-, 2,7-, 3,6- and 4,5-$DMeC_8$, 4-EC_8 and 5-EC_8 compounds. By using commercial naphtha containing important amount C_4 and C_6, the molecular weight distribution of the product is broadening (Figure 10 complementary information).

The product distributions shown in Table 2 (obtained at ~90% conversion) are different from those reported by Schmidt et al. (2008) [6] on mordenite and those reported for pentene dimerization on a phosphorous catalyst (Kolesnikova et al. [25]). The octane numbers of C_{7-15} measured on products were around 95, proving their value as gasoline components.

3.1.2. Spent catalyst

The spent catalyst after one week on stream at 470 K had lost 37% of the surface and 30% of total pore volume (91% of micropores). The catalyst had accumulated a low amount of coke (~4.5%), and had lost 80% of the acid function detected by pyridine and 44% of metal detected by CO adsorption. All of that resulted in 55% reduction in activity. In a previous paper [8], we had shown that carbon deposition – which eliminated the major part of microporosity – is accumulated during the first hour on stream, and the total amount did not correlate with the loss of catalyst activity as a function of time on stream. The dimerization occurred in the mesopores where the paraffins molecules have no constraint to deeply isomerize into di- and tri-branched compounds. Table 2 shows an example of the product distribution formed at 450 K with the used catalyst (after isothermal operation for one week). The product distribution is still centered on C_{10} hydrocarbons. IR analyses of spent catalysts show that most of the carbonaceous deposits contain aromatic molecules that remain adsorbed (small bands at 3310 and 3094 cm^{-1} due to CH stretching and two intense bands at 1470 and 1080 cm^{-1} due to the methylene group (=CH_2)), which was confirmed by the presence of bands at 160 and 120 ppm in solid ^{13}C NMR analyses. Therefore, for these catalysts, a slow rate of dehydrogenation–condensation of the adsorbed dimer intermediary (cyclo-carbonion) that produces a minute amount of naptho-aromatics deposits was observed. The latter reduced the number of mesoporous acid sites in similar way to those observed by us on Pt/mordenite, and reported on PtGaZr/Si [7], and $PtSO_4Zr$ [26]. The first step in the coke build up occurs by condensation of the adsorbed carbonion dimers into cyclo-intermediaries; then the latter are dehydrogenated into naphtho-aromatics type compounds (still xylene-soluble hydrocarbons). These on-surface compounds "aged" into coke by dehydrogenation and cracking as a function of time on stream, becoming xylene-insoluble deposit (coke). The presence of Pt and hydrogen limits the further condensation and dehydrogenation of the intermediates into aromatics. The coke built up reduce 20% the effective diffusivity but do not plug the mesoporous structure (Table 1). When the reaction temperature increases, slightly augments the rate of aromatization of the carbonaceous deposit, thus coke starts to accumulate on catalyst with the subsequent deactivation of the catalyst.

3.1.3. Regenerated catalyst

After regeneration at the laboratory scale, the catalyst had recuperated 80% of the surface area, 90% of the pore volume, and only 58% of the micropores. Coke was still present on the solid, but 60% of the acidity measured by pyridine and 88% of the metal measured by CO adsorption were recovered; all of that resulted in an activity of 0.92% with respect to fresh catalyst (Table 1). The level of conversion of C_5 into C_{10} for spent catalyst depends on the regeneration conditions used; the values reported in Table 2 correspond to the first cycle of regeneration; information for the next cycle reaction-regeneration is under development. For the following simulation, we will assume that the same activity will be

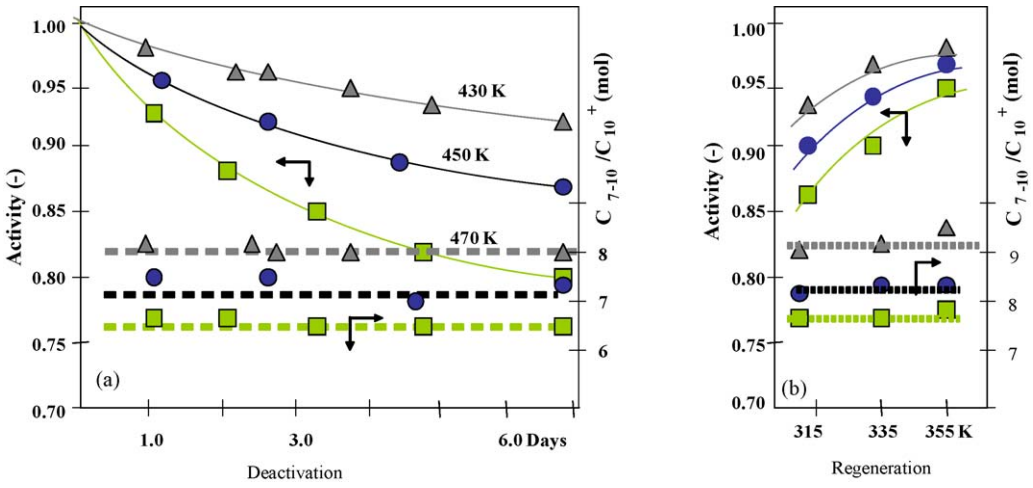

Fig. 2. (a) Isothermal catalyst deactivation and selectivity for seven days: at 430 K (▲), 450 K (●) and 470 K (■), space velocity of 1.0 h^{-1}, pressure of 0.8 MPa and H_2/HC ratio of 0.022 (mol); (b) activity and selectivity after regeneration the catalyst deactivated at (▲) 430 K, (●) 450 K and (■) 470 K; operating conditions and regenerated at 315, 335 and 355 K for 5 h followed hydrogen treatment.

recovered after all regeneration cycles. The GC–MS analysis of the xylene extracts shows the presence of aromatics and naptho-aromatics (2% of alkylbenzenes, 7% of alkyl tetralins, 20% alkyl-naphthalenes, and 10% indanes, among others heavy molecules). Spectroscopy analysis of regenerated catalyst shows a strong reduction in the bands at 1470 and 1080 cm^{-1} (IR) as well as in those at 180–140 ppm (^{13}C NMR) already observed on the spent catalyst. Longer the time on stream and higher the temperature used in the operation, lower is the effect of xylene extraction on catalyst regeneration due to the aging of deposit into coke. The regeneration improves the access to the microporous and the effective diffusivity increases (Table 2) to a near the fresh catalyst value.

3.2. Catalyst deactivation and regeneration simulation

The average activity of the catalyst during the one-week tests is shown in (Fig. 2a) as a function of time on stream, calculated using the previous kinetic model (Table 3) and the values of the deactivation rate parameters (Eq. (18) k_d: 10^{12} d^{-1} and E_d: 117.15 kJ/mol). These kinetics and deactivation parameters were verified by comparing the prediction of the products concentration by the model with the data obtained in the three currents tests. Fig. 3 shows for a set of 21 data points (three tests of seven days at three temperatures) that the simulation model is able to predict the amount of nC_{10} formed within less than 1.5% error. The model also calculated well the average isomerization (iC_i/nC_i) ratio determined by ^{13}C NMR (see the comparison inside Fig. 3).

Fig. 2a indicated a progressive deactivation of the catalyst as a function of time on stream at quasi-constant selectivity (C_{7-10}/C_{10}^+) in the range of pentane conversion studied here and for three deactivation temperatures; these results confirm that only one kind of active site is involved for all dimerization and trimerization reactions. The effective diffusivity is also reduced with respect to the fresh catalyst but no indication of pore mouth blockage was observed. Therefore, deactivation occurred by reduction of the number of these active sites. Similar deactivation of acid sites were observed for a naphtha reforming catalyst [20], but the effect of temperature in deactivation is higher than observed in a C_5 commercial isomerization plant (Pt/mordenite, not shown). Schmidt et al. [6] tested different Si/Al ratios in mordenite 40 and observed stability at 55% conversion of olefins for 400 h of light naphtha dimerization by increasing the temperature from 423 to 473 K at 3 MPa of pressure. Their results correspond to lower deactivation energies for C_5 dimerization than those measured by us in hydrogen and they were obtained with a catalyst completely different in structure, acidity, and composition. The reduced effect of temperature in selectivity is due to small (relative) differences in specific activation energies (Table 3) between the main reactions, and to the narrow carbon number distribution in the product (composition dominated by dimerization of iso-pentene – the fastest reaction – into di-branched decanes).

The regeneration occurred by extraction of small amount of the naptho-aromatic polymers formed during the dimerization reaction that remain adsorbed. The analysis of the xylene-washed catalysts indicates that the amount of carbon on surface decreases as a function of time on stream (see complementary information). Higher the extraction, higher is the activity (a quasi-constant selectivity). This favorable effect of temperature is attributed to the higher polymer solubility in xylene. In fact a solid deposit is formed when the xylene extracts were cooled to room temperature. Fig. 2b shows the recovery of activity (right axis) at constant selectivity (left axis) after 5 h of xylene washing and ulterior hydrogen treatment. The maximum temperature used for solvent regeneration depends on the need to have liquid phase in the reactor at 0.8 MPa, which is the same than those used for dimerization reactions. For that the reactor is cooled down (315–355 K) to proceed with the regeneration and then reheated to come back into dimerization operation, a process that uses more time than the regeneration itself. The deactivation results can be simulated by Eq. (20) using the following constants: k_{reg}: 10^7 d^{-1}, and E_{reg}: 41.84 kJ/mol. Table 2 indicates that

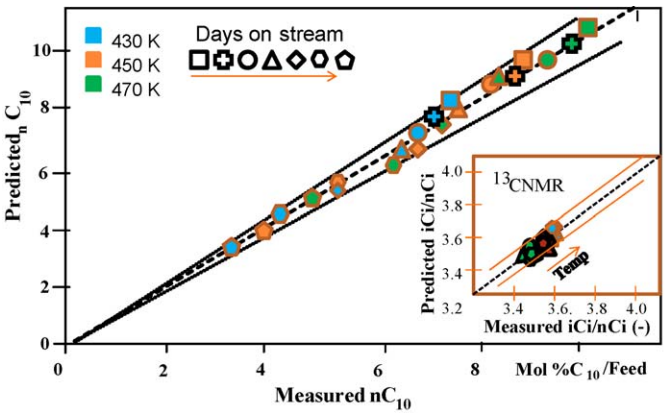

Fig. 3. Prediction by the model of the amount of nC_{10} and the isomerization index (average iso/nC_i ratio) in the product versus data measured during one-week test at 430, or 450 or 470 K. The points represent the analyses of daily sample.

after regeneration at 355 K, the catalyst still contains 0.1% of carbon, and the analysis of carbon as a function of time (see supplementary information) does not correlate with activity recovery, proving that most of the carbonaceous material, early on time deposited on spent catalysts, has no effect on activity.

Having the kinetic, deactivation, and regeneration rate parameter, the commercial process scheme could now be simulated to determine the best cycle of operation for the reactors.

3.3. Base case and process simulation

3.3.1. Base case

Fig. 1 shows the general scheme for the process composed by a heater, two reactors operating in parallel, a cooling and separation of effluents, a recycle of hydrogen and fractionation of the products. Table 4 shows the input and output data used by the model. The program had the capability to work in different modes of operation for the reactor with and without recycle of unconverted naphtha. To be able to compare performances, a simple base case was established, after which, several simulations were performed by varying one of the operational parameters with respect to the base case. In the base case a light naphtha, with a composition similar to that depicted in Table 2, was dimerized in one adiabatic reactor with three hydrogen quenches using 450 K as constant inlet temperature, 1 h^{-1} space velocity, 0.8 MPa of total pressure, a 0.03 H_2/HC ratio, and a maximum delta of temperature in the beds of 20 K adjusted by hydrogen quenches. The end of run occurred when the average activity attained a value of 0.5. Then this reactor is regenerated and the standby reactor comes up on stream. Based on our experience with a commercial isomerization plant, almost two days were needed for adjusting the temperature in the plant for washing the catalyst with reformate (gasoline) at 375 K, and another three days are needed for heating back the reactor in hydrogen to 450 K. The minimum time out of the stream to regenerate the catalyst is around one week.

Fig. 4 shows for the base case the activity and the selectivity predicted by the model along the reactor bed at the start of run. The rise in temperature along the bed is due to the exothermic hydrogenation reactions. This increment in temperature preferentially accelerates the hydrogenation and isoparaffins dimerization than trimerization and other reactions, increases cracking reactions and reduces the $ii C_i/iC_i$ ratio. The initial product distribution for the base case showed 85% selectivity to C_{7-10}, mostly isoparaffins and naphthenes, for around 90% total C_5 conversion. The hydrogen used in the quenches increments the hydrogen concentration and reduces the hydrocarbon concentration, as well as reduce the increment of temperature along the reactor, causing discontinuities in the profile of concentrations (recalculated after each H_2 addition). Heaviest products are produced in series by trimerization and polymerization reactions, giving hydrocarbon products that boil above the naphtha fraction range (C_{11}^+) and causing deactivation; for that the conversion of C_5 has to be limited to 80–90% depending on temperature used. It should be noted that this catalyst converts not only olefins but also dimerized paraffins, which is an advantage, but it experiences higher deactivation than Pt/mordenite isomerization catalyst. The simulation of the adiabatic reactor operation at constant inlet temperature shows that the accumulation of this carbonaceous deposit produced an important reduction in activity (Fig. 5, right axis) and the concentration of the C_{7-10} product is reduced as a function of time on stream (Fig. 5, left axis). The rate of deactivation changes along the reactor with olefins, hydrogen and temperature but the profile of activity is dominated by the latter. Fig. 5 (bars) shows that due to deactivation, the delta of temperature in the quench zone is reduced as a function of times on stream in the two

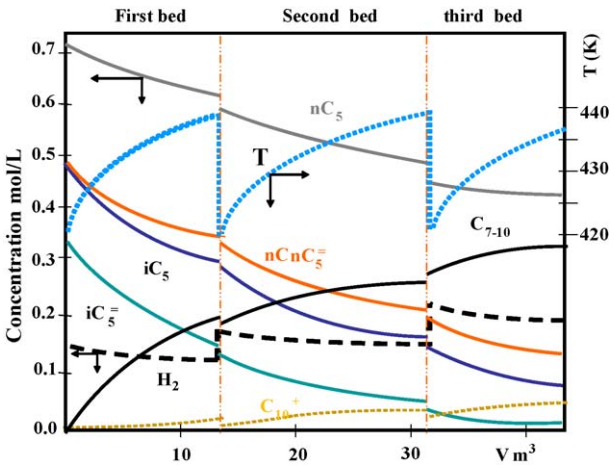

Fig. 4. Base case. Simulation of the concentration profile (gas phase) for the base case operating conditions and $t = 0$ for the three reactor beds: solid lines left axis \ nC_5, \ iC_5, \ $nC_5^=$, \ $iC_5^=$, \ C_{7-10}, dashed lines left axis – C_{10}^+, and – H_2, dotted lines (right axis) • • • Temperature profiles.

quenches, for the same inlet temperature in the beds; the amount of hydrogen needed after the second bed to cool down the gas to the inlet temperature is higher than those needed after the first bed due to the additional hydrogen incorporate in gas in the first quench. In general, by using a constant inlet temperature along the cycle length, the conversion and the production of C_{7-10} components decreases as a function of time on stream, as does the total hydrogen required in the quenches. The catalyst in this reactor is then regenerated during one week and comes back in operation when the catalyst in operation is deactivated; each reactor operates during 4.3 periods in a year. The annual production for the base case generates a relative low benefit using the 2004 fuel prices (0.1 $/bbl). The uses of two reactors in parallel, out of phase for one week improve the benefits (0.17 $/bbl) in spite of the higher investment.

The isothermal operation can be performed at lower initial temperature but similar conversion. That extends the time in reaction and decreases the number of regeneration needed per year, increases the investment, slightly reduces the selectivity, and improves the margin (0.22 $/bbl). The principal conclusion in this part is that by working with the two reactors out of phase at low and constant inlet temperature reduces the losses associated with the time out of stream for regeneration. Fig. 6 shows that higher the initial temperature used in the reactor, larger the C_{7-10}

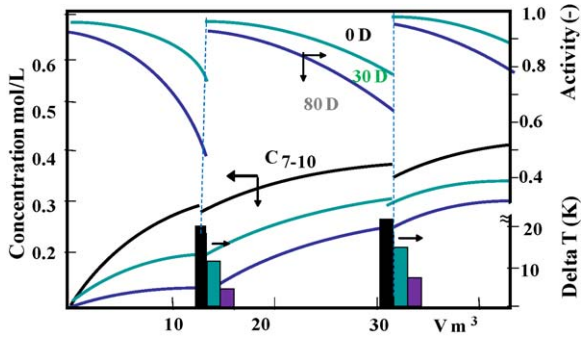

Fig. 5. Base case. Simulation of the effect of time on stream on activity (solid lines right axis, \ 0, \ 30 and \ 80); on concentration of C_{7-10} (solid line – left axis, \ 0, \ 30 and \ 80D on delta of temperature at the quench zone (bars – right axis, r ■ 0, ■ 30, and ■ 80 D. One adiabatic reactor on stream with constant inlet temperature and two intermediate quenches.

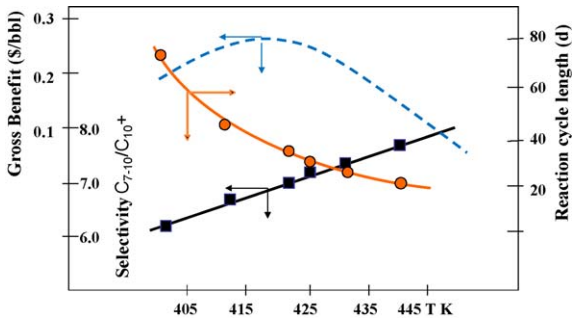

Fig. 6. Base case. Effects of temperature on gross benefit (▬ left axis), selectivity (■ left axis) and reaction cycle length (● right axis).

hydrocarbons production (left axis), but shorter the time on stream (right axis), which is dramatically reduced by the acceleration of catalyst deactivation. The benefit is affected by the additional investment and the number (and cost) of regenerations. The benefit increases from 400 to 415 K due to a reduction in reactor volume, then passes by a maximum for an inlet temperature of 415 K and decreases at higher temperature by the cut down of the time on stream. Since the activation energies are lower than the deactivation energy different options mentioned in the literature can be used to compensate for the deactivation: increase the temperature or/and decrease the throughput.

3.4. Reactor operation optimization

3.4.1. Effect of increasing temperature along the cycle length

There are different strategies for increasing the temperature, having quenches in the reactor, which can maximize gasoline production at minimum operating cost (maximum benefit). The relative temperature dependency of the rate of reaction, deactivation, and regeneration are the main factors in setting the optimal operation. For example, one option is to start at the same initial temperature in the three beds and increase these temperatures along the cycle length in a way to have constant average activity in the three beds; thus, the C_5 conversion remains constant along the cycle, while the selectivity is slightly improved and the stability of the catalyst is continuously deteriorated. This is carried out by increasing the first bed inlet temperature more than the second and third bed. The larger deactivation of the first bed is due to the higher concentration of olefins and lower of hydrogen than those existing in the following beds. In this mode of operation the amount of hydrogen added in the two beds remain quite constant along the cycle. The time on stream is drive for the maximum temperature in the first bed. Other possibility is to start at the same inlet temperature in the three beds and then increase simultaneously the inlet temperature of the three beds at the same level along the time on stream; this mode of operation produces a progressive enlargement of the third bed average activity with respect to the second and the first ones; it occur a transfer of non converted C_5 from the first to the second and then to the third bed. Now the amount of hydrogen added after the second quench increases more than that in the first one as the cycle progresses. The third possibility is to start the cycle with different inlet temperature in each bed and increase initial temperatures as the cycle progresses following a particular ratio of beds' temperatures (pattern shown in Eq. (28)). This mode of operation uses more volume of catalyst in the first bed (the coolest one) and less in the third one (the hottest one) than previous option. The latter mode improves the benefit (0.28 $/bbl) respect to the base case.

3.4.2. Effect of using two out of phase reactors with a programmed beds inlet temperatures profile

The two identical reactors start the operation at different inlet temperatures (~10 °F) but with the following ratio of beds' temperatures:

$$T_{\text{First bed}} : 0.9T_{\text{Second bed}} : 0.8T_{\text{Third bed}} \quad (28)$$

The reactor I uses a high inlet first bed temperature for over-converting the feed to compensate the under-converting of reactor II that employs a low first bed initial temperature. The profile of inlet beds' temperatures in both reactors follows the proportion indicated by Eq. (28); then the three temperatures (at constant ratio) are differently increased in both reactors as a function of time on stream to keep C_5 conversion constant. When the reactor (I) arrives to the maximum allowed temperature, it goes out of stream and it is regenerated for one week, while reactor (II) continues processing half of the feed at the same conversion used before. After the regeneration, reactor I comes back in operation and starts its new cycle at over-converting conditions, while reactor II continue its operation at under-converting conditions, each on processing half the throughput. When reactor II arrives to the maximum temperature it goes to regeneration while reactor I keep on operation. The cycle continues with two reactors operating with one week out of phase, at different inlet temperatures. In this scheme, during the regeneration the production and the benefits are reduced. The program was run with other combinations to determine the best progression in temperature for the two reactors that maximize the annual C_{10} production or the benefit. The minimum down time that the reactor required for regeneration depends more on the time required for adjusting the temperature than on the rate of regeneration. For that there is a limited opportunity to improve the benefits by changing the regeneration conditions. The above mentioned operation of the system can be extended by using a swing mode of operation for three reactors to keep the production constant at the expense of higher investment (higher reactor volume), like in semi-regenerative reforming of naphtha. Thus, two reactors out of phase can be operated in parallel and the spare reactor comes on stream when one of the reactors goes into regeneration. It should be noted that regeneration by solvent and hydrogen could be done at the same operating pressure than that used during normal operation. The present regeneration is two or three weeks shorter than that of the carbon burning technology. The plot of the activity and selectivity using a programmed inlet temperature is similar to those previously shown in Fig. 5.

The same optimization study was done by changing the H_2/HC ratio and the level of conversion per pass with recycle of unconverted C_5 paraffins.

3.4.3. Optimal economic plant operation

The general balance for the plant (depicted in Fig. 1) can be seen in the thesis of Albornoz Hernández [27], which shows details about the equipments' calculations and capital and operational costs, broken down by equipments. In summary, the analysis of how the variables affect the investment indicated that the main contribution in total investment cost is from the capacity of hydrogen compressors (40%), followed by the volume of the reactor (18%), the heat exchangers (15%) and the high-pressure pumps (10%). The main operating cost contributions are the feed (70%) followed by hydrogen (15%), and electricity (5%). The optimum cycle length was found to strongly depend on the production losses during the regeneration, and the progression of temperature used in the reactors.

3.4.4. Mass and heat transfer

The program had verified that there is no effect on the rate of reactions from mass and heat transfer to, into, and from the catalyst particles (Eqs. (25)–(27)); thus, the present mass and heat balance equations represent the apparent behavior of the catalyst particles.

4. Conclusions

A PtGaZr/Si catalyst performance for the dimerization of light cracked gasoline in a swing type reactor was mathematically simulated using a lump of 32 reactions, a one-site deactivation model, and a regeneration rate model. The kinetic, deactivation, and regeneration rate constants were experimentally determined. The results show the following:

- The catalyst is 86% selective for the C_{7-10} dimers formation at around 90% of C_5 conversion operating in gas phase at temperatures around 450 K, space velocity around 1, and a H_2/HC ratio of 0.03. The reactions produce small amount of trimers, cycloparaffins and cracked products, but none of the aromatics and olefins are present in the product. At this conversion and low temperature the catalyst moderately deactivates by carbonaceous deposits and it can be partially regenerated by xylene extraction and hydrogen treatment.
- The augment in reactor temperature increases the catalyst deactivation, slightly improves the selectivity and reduces the level of isomerization, thus the octane number.
- The catalyst was deactivated by accumulating some naptho-aromatics, soluble in xylene compound, on surface which reduces its acidity, metal dispersion and iC_5 diffusivity but does not proportionally reduce its activity.
- The rate of catalyst regeneration increases with temperature and contact time. The extraction with xylene and ulterior hydrogen treatment recover most of the iC_5 effective diffusivity, acid sites and metal dispersion and more than 90% of original activity by reducing the on-surface concentration of adsorbed naptho-aromatics. Small amount of coke remains in micropores after regeneration.
- The simulation program developed is able to predict the yields and product quality as a function of time on stream in a light naphtha dimerization process. For the simulation the program uses a lump of 32 apparent kinetic rate equations, one rate equation for deactivation and another for regeneration and the kinetic, deactivation, and regenerations parameter obtained from experimental data.
- The gross benefits of the process could be improved by using two or three swing multi-bed adiabatic reactors system operating with a week out of phase and by programming the increase in bed inlet temperature along the cycle length.

Acknowledgements

The authors would like to acknowledge the experimental work of Eng. P. Bonilla, the debugging of the simulation program done by Eng. Edgar Santillan, and Simon Bolivar University (Venezuela) for the economical support.

Appendix A. Supplementary data

Supplementary data associated with this article can be found, in the online version, at doi:10.1016/j.cattod.2009.10.013.

References

[1] E. Lutz, G. Bailey, Selective polymerization of 1-pentene in presence of 2-methyl-1.butene, J. Polym. Sci., Part A-1 4 (1966) 1985–1986.
[2] N.G. Polyanski, E. Tsekhmister, Catalytic polymerization of C_5 olefins in the presence of sulfonated cation exchange resins, Neftekhimiya 4 (2) (1964) 262–268.
[3] M. Hochtl, A. Jentys, H. Vinek, Isomerization of 1-pentene over SAPO, CoAlPO (AEL, AFI) molecular sieves and HZSM-5, Appl. Catal., A 207 (2001) 397–405.
[4] D. Rutembeck, H. Papp, H. Ernst, W. Schwieger, Investigations on the reaction mechanism of the skeletal isomerization of *n*-butenes to isobutene: Part I. Reaction mechanism on H-ZSM-5 zeolites, Appl. Catal. 205 (2000) 57–63.
[5] S. Miller, R. Krug, Two stage dimerization of C_5–C_{11} alkene fractions for production of base stocks for lubricating oil, World Patent WO 2002055633 (2002).
[6] R. Schmidt, M. Bruce, B. Randolph, Oligomerization of C_5 olefins in light catalytic naphtha, Energy Fuels 22 (2008) 1148–1155.
[7] J. Bonilla Platin, R. Galiasso Tailleur, Kinetic of Light naphtha dimerization, Simón Bolívar report 47723-07, unpublished results (1997).
[8] R. Galiasso Tailleur, J. Bonilla Platin, Role of Pt on PtGaZr/SiO_2 catalyst in light naphtha isomerization, J. Catal. 255 (2008) 79–93.
[9] R. Bacaud, S. Gamez, M. Vrinat, Aging of industrial hydrotreating catalyst, in: Preprint 230th ACS Div of Petroleum Chemistry, vol. 50, no. 4, 2005, 375–377.
[10] N. Mohsen Harandi, O. Hartley, Method for on-stream low-pressure regeneration of an oligomerization catalyst from a fluid-bed reactor operating at high pressure with hydrocarbons in a non-liquid phase, US Patent 4939314 (1990).
[11] M. Mariochionna, M. Di Girolamo, R. Patrini, Light olefins dimerization to high quality gasoline components, Catalyst Today 65 (2001) 397–403.
[12] R. Frame, L. Stine, H. Hammershaimb, B. Muldoon, High octane gasoline from field butanes by the UOP indirect alkylation (InAlk) process, Erdoel, Erdgas, Kohle 114 (7–8) (1998) 385–387.
[13] J. Chen, Z. Ring, T. Dabros, Modeling and simulation of a fixed bed pilot plant hydrotreated, Ind. Eng. Chem. Res. 40 (2001) 3294–3300.
[14] A. Savoretti, D. Borio, V. Bucalá, J. Porras, Non-adiabatic radial flow reactor for styrene production, Chem. Eng. Sci. 54 (1999) 205–213.
[15] W.J. Lee, G.F. Froment, Ethylbenzene dehydrogenation into styrene: kinetic modeling and reactor simulation, Ind. Eng. Chem. Res. 47 (2008) 9183–9194.
[16] A. Takashi, in: A. Takashi, P.L. Silveston (Eds.), Cyclic Separating Reactors, 2007, Print ISBN: 9781405131568, Online ISBN: 9780470988688, doi:10.1002/9780470988688.
[17] Ch. Lee, Ch.H. Fan, P.-F. Yang, Modeling and simulation of a pressure swing reactor for the conversion of poorly soluble substrate by immobilized enzyme: the case of D-hydantoinase reaction, Biochem. Eng. J. 7 (3) (2001) 233–239.
[18] P. Heidebrecht, C. Hertel, K. Sundmacher, Conceptual analysis of a cyclic water gas shift reactor, Int. J. Chem. Reactor Eng. 6 (2008).
[19] N. Nikolaou, C.E. Papadopoulos, I.A. Gaglias, K.G. Pitarakis, A new non-linear calculation method of isomerisation gasoline research octane number based on gas chromatographic data, Fuel 83 (4–5) (2004) 517–523.
[20] O. Levenspiel, Chemical Reactions Engineering, second edition, REPLA, s.a. Editorial, 1987.
[21] R. Galiasso Tailleur, Y. Davila, Optimal hydrogen production through revamping a naphtha-reforming unit: catalyst deactivation, Energy Fuel 22 (5) (2008) 2892–2901.
[22] L. Pellegrini, S. Gamba, S. Bonomi, V. Calemma, Equilibrium constants for isomerization of *n*-paraffins, Ind. Eng. Chem. Res. 46 (16) (2007) 5446–5452.
[23] R. Galiasso Tailleur, Effective diffusivity measurement in coke-deactivated hydrotreating catalyst, Preprint of the WCCE-8 Congress held in Montreal, August (2009).
[24] G.F. Foment, K. Bischof, Chemical Reactor Analysis and Design, John Wiley & Sons, New York, 1979, ISBN 0-471-02447-3, pp. 394–357.
[25] T. Kolesnikova, M. Kolbin, R. Kayumov, L. Krasnova, A. Grudnikova, Structure of products from pentene polymerization on phosphorous catalyst, Neftepererabotka i Neftekhimiya 1 (1970) 27–28.
[26] S.R. Vaudagna, R. Comelli, S. Canavese, N. Figoli, SO_4/ZrO_2 and $Pt/SO_4/ZrO_2$: activity and stability during *n*-hexane isomerization, J. Catal. 169 (1997) 389–393.
[27] C. Albornoz Hernández, Simulacion de una planta de dimerization de nafta liviana en un reactor FPIP con desactivacion, MSc thesis Simon Bolivar University, Caracas Venezuela, 2004.